AIP | The Journal of Chemical Physics

Entropy production in a mesoscopic chemical reaction system with oscillatory and excitable dynamics

Ting Rao, Tiejun Xiao, and Zhonghuai Hou

Citation: J. Chem. Phys. **134**, 214112 (2011); doi: 10.1063/1.3598111
View online: http://dx.doi.org/10.1063/1.3598111
View Table of Contents: http://jcp.aip.org/resource/1/JCPSA6/v134/i21
Published by the American Institute of Physics.

Additional information on J. Chem. Phys.

Journal Homepage: http://jcp.aip.org/
Journal Information: http://jcp.aip.org/about/about_the_journal
Top downloads: http://jcp.aip.org/features/most_downloaded
Information for Authors: http://jcp.aip.org/authors

ADVERTISEMENT

Downloaded 23 May 2013 to 129.186.1.55. This article is copyrighted as indicated in the abstract. Reuse of AIP content is subject to the terms at: http://jcp.aip.org/about/rights_and_permissions

Entropy production in a mesoscopic chemical reaction system with oscillatory and excitable dynamics

Ting Rao, Tiejun Xiao, and Zhonghuai Hou[a)]
Hefei National Laboratory for Physical Sciences at Microscale and Department of Chemical Physics, University of Science and Technology of China, Hefei, Anhui, 230026, People's Republic of China

(Received 16 March 2011; accepted 18 May 2011; published online 7 June 2011)

Stochastic thermodynamics of chemical reaction systems has recently gained much attention. In the present paper, we consider such an issue for a system with both oscillatory and excitable dynamics, using catalytic oxidation of carbon monoxide on the surface of platinum crystal as an example. Starting from the chemical Langevin equations, we are able to calculate the stochastic entropy production P along a random trajectory in the concentration state space. Particular attention is paid to the dependence of the time-averaged entropy production P on the system size N in a parameter region close to the deterministic Hopf bifurcation (HB). In the large system size (weak noise) limit, we find that $P \sim N^{\beta}$ with $\beta = 0$ or 1, when the system is below or above the HB, respectively. In the small system size (strong noise) limit, P always increases linearly with N regardless of the bifurcation parameter. More interestingly, P could even reach a maximum for some intermediate system size in a parameter region where the corresponding deterministic system shows steady state or small amplitude oscillation. The maximum value of P decreases as the system parameter approaches the so-called CANARD point where the maximum disappears. This phenomenon could be qualitatively understood by partitioning the total entropy production into the contributions of spikes and of small amplitude oscillations. © *2011 American Institute of Physics*. [doi:10.1063/1.3598111]

I. INTRODUCTION

Very recently, stochastic thermodynamics (ST) has gained considerable attention, ever since the pioneer work of Udo Seifert and co-workers.[1–7] ST provides a framework for describing small systems, such as colloids or biomolecules, driven out of equilibrium but still in contact with a heat bath. A first-law like energy balance involving exchanged heat and work done, as well as entropy production entering the refinements of second law, can be defined consistently along a stochastic trajectory. Importantly, some general fluctuation relations hold for these stochastic trajectory-based thermodynamic variables. The total entropy change, Δs_{tot}, is shown to be related to the dynamical irreversibility of the trajectory. It also obeys the so-called integral fluctuation theorem (FT), $\langle \exp(-\Delta s_{tot}) \rangle = 1$, which gives the second law $\langle \Delta s_{tot} \rangle \geq 0$. In nonequilibrium steady states, a detailed form of FT also holds for Δs_{tot}, i.e., $p(\Delta s_{tot})/p(-\Delta s_{tot}) = e^{\Delta s_{tot}}$, where $p(\cdot)$ denotes the probability that Δs_{tot} takes a certain value. Albeit ST was originally applied to Brownian particles described by over-damped Langevin equation, the concepts and principles can also be applied to general stochastic systems described by master equations. Although first-law like energy balance should be properly interpreted for general stochastic dynamic systems, trajectory-based entropy production can be well-defined, such that second-law and FT can be well established. Such approaches may lead us closer towards a systematic understanding of nonequilibrium statistical mechanics of small systems, in general. In this context, ST has found wide applications in optically driven colloids,[4] (bio)chemically driven enzymes,[7] state transition in biomolecules,[7] general chemical reaction networks,[6] to list just a few. In fact, the stochastic theory of small chemical systems, especially chemical master equation (CME), has been a significant and important topic since the pioneer works of Leontovich,[8] Delbrück,[9] and McQuarrie.[10] (Comprehensive reviews on this topic can also be found in Ref. 11 and references therein.) Since then, many approximate methods[12–15] based on CME, have been developed to investigate the stochastic dynamics[16,17] and thermodynamics[18,19] of chemical reactions. It is worthy to note that, based on CME, there is also another kind of framework, provided by Gaspard and co-workers[20–24] to investigate nonequilibrium thermodynamics and dynamic irreversibility in small systems, where a trajectory-based functional $Z(t)$, is introduced to describe the dissipation of a chemical reaction system in nonequilibrium steady state.[21] The authors have further demonstrated that the statistical average $\langle Z(t) \rangle$ of functional $Z(t)$ over the path could be related to the entropy flow as defined by Nicolis and co-workers.[19]

In two recent papers, we have applied ST to mesoscopic chemical oscillation systems with supercritical Hopf bifurcations (HB).[25,26] Our main motivation is to unravel the interplay between the nonlinear dynamic behaviors far from equilibrium and ST features. We first considered the conceptual Brusselator model, described by a master equation. Although the reactions are irreversible, the transitions in the molecular number state space are reversible, which serves as a kind of micro-reversibility based on which time-reversed trajectory can be well defined. We have calculated the entropy production P along a stochastic limit cycle by using Gillespie algorithm, in a parameter region close to the HB. Interestingly,

a)Electronic mail: hzhlj@ustc.edu.cn.

 © 2011 American Institute of Physics

Downloaded 23 May 2013 to 129.186.1.55. This article is copyrighted as indicated in the abstract. Reuse of AIP content is subject to the terms at: http://jcp.aip.org/about/rights_and_permissions

P shows distinct scaling behaviors with the system size V at different side of the HB: it increases linearly with V in the deterministic oscillatory region, while it is independent of V in the steady state region. Such an observation implies that one may use ST features to characterize the occurrence of a HB, which can be viewed as a kind of nonequilibrium phase transition, in mesoscopic chemical systems. To further demonstrate this, we later extended our study to a general reaction network, described by chemical Langevin equations (CLE). Herein, the reversibility is related to the continuous concentration space and requires only at a coarse-grained level, much more relaxed than that in the molecular-number space. This time, the entropy production along a stochastic trajectory can be calculated by using a path-integral approach. Thanks to the stochastic normal form theory we developed before to account for noise-induced oscillation and coherence resonance,[27,28] we were able to obtain the analytical expression for P when the system is close to HB. The analysis clearly showed that P scales as V^{α} in the limit $V \to \infty$, where α equals to 0, 0.5, or 1 when the system is below, at, or above the HB, respectively. These two studies shed some new lights on the application of ST in characterization of typical nonlinear dynamic features, where the oscillation associated with HB.

In the present paper, we continue these series of studies to a mesoscopic chemical reaction system with both oscillatory and excitable dynamics. Excitability is of ubiquitous importance in many physical, chemical, and biological systems. It describes any stable dynamical system that exhibits pulses when the amplitude of a perturbation exceeds a fixed threshold. In spatially extended systems, this leads to the generation of fronts and spiral waves, most notably occurring on surface catalytic reactions on single crystal surfaces and on human heart leading to fibrillation.[29–34] Excitability usually involves time-scale separation in the dynamic evolutions of a fast and a slow variable. In case when both oscillatory and excitable dynamics coexist in a system, two types of oscillations can be observed: one is quasi-harmonic oscillation with small amplitude growing from the HB, the other is relaxation oscillation with large amplitude and multi-time scales. In such systems, small oscillations may change abruptly to large spikes in an exponentially narrow parameter regime, known as CANARD phenomenon. Following our previous studies, we are thus wondering how such nontrivial dynamic features would influence the ST properties, especially the scaling behaviors of the entropy production.

To this end, we have applied the concept of ST to a model system, carbon monoxide (CO) oxidation on platinum (Pt) surface. We choose this system for twofold reasons. On one hand, CO oxidation systems are of both theoretical and experimental interests, our study may help understand the nonequilibrium fluctuation properties of this important system. In heterogeneous catalysis, sufficiently small systems to be strongly influenced by internal noise are provided by the facets of a field emitter tip,[35] by nanostructured composite surfaces,[36] and by the small metal particles of a supported catalyst.[37] It was found that internal noise can induce transitions between the active and inactive branch of the reaction for catalytic CO oxidation on a Pt field emitter tip.[35] Internal noise becomes essential in the dynamic behavior of CO oxidation when surface cells over low-index single crystal surface are very small.[17] Using FIM/FEM, the researchers have investigated the imaging of a catalytic reaction on an atomic scale.[38–40] The experimental study has also shown that coverage fluctuations on catalytic particles can drastically alter their macroscopic catalytic behavior, causing bistability to vanish completely with decreasing particle size.[41] Using a stochastic model[37,42,43] Peskov and co-workers demonstrated that the large difference between the oscillations observed on a 4-nm and 10-nm Pd particles was a consequence of the interplay between the system's nonlinear dynamics and the internal noise. When the pressures are higher, a realistic atomistic model[44] is needed to assess spatiotemporal behaviors including the influence of fluctuation and adspecies interactions in nanoscale CO oxidation systems. On the other hand, very abundant nonlinear dynamic behaviors[17,45–49] have been observed in this system, including multistability, oscillation, excitability, as well as CANARD phenomenon. We consider that the surface is divided into many mesoscopic cells, whose space scale is determined by the diffusion length. The reactions inside each cell are considered to be homogeneous, while concentration gradient may exist between neighboring cells. For simplicity and as the first step, in the present work, we only consider the behavior inside a single cell[35,50] just like the disposal by Eiswirth *et al.*[17] Extension to spatially extended systems might be possible in principle[3] but is beyond the scope of the present study.

We start from the CLE describing the dynamics inside a cell containing N lattice sites. By using path integral approach, expressions for the entropy production P can be obtained, which depend on the detailed dynamics along a stochastic trajectory. We focus on a parameter region close to the deterministic Hopf bifurcation, and particular attention is paid to the dependence of P on the system size N, here denoting the number of lattice sites inside a mesoscopic surface cell. Our numerical results show that P always increases linearly with N when N is small, regardless of the control parameter. In the large N limit, however, P may scale as N^1 or N^0 depending on the parameter value. In the intermediate range of N, P can even show a maximum. By partitioning P into two parts, one contributed from the spikes and the other from small amplitude oscillations, and investigating the dependences of both parts on N separately, we can then qualitatively illustrate the scaling laws of P and the occurrence of the maximum.

II. MODEL AND RESULTS

The model used in the present paper was developed for the oxidation of CO on Pt(110) on single crystal surface.[17] The reaction follows a Langmuir-Hinshelwood mechanism, which involves the adsorption of CO and O_2 molecules, desorption of CO molecule, and the reaction between adsorbed CO molecule and O atom. In addition, the adsorbate-induced $1 \times 1 \Leftrightarrow 1 \times 2$ phase transition is taken into account to address the influence of the surface structure on the reactivity. The state of a cell containing N adsorption sites can be described by $X_N(t) = [N_{\mathrm{CO}}(t), N_O(t), N_{1\times1}(t)]^T$, where N_{CO}, N_O, and $N_{1\times1}$ denote the number of adsorbed CO molecules,

Downloaded 23 May 2013 to 129.186.1.55. This article is copyrighted as indicated in the abstract. Reuse of AIP content is subject to the terms at: http://jcp.aip.org/about/rights_and_permissions

TABLE I. Stochastic processes and reaction rates for CO oxidation on Pt(110). The meaning of physical quantities is listed in Table II, and corresponding parameter values are the same as those listed in Table II of Ref. 17.

Process	Rate	Descriptions
$N_{CO} \to N_{CO}+1$	$a_1 = NP_{CO}k_{CO}S_{CO}(1-u^{\xi})$	CO adsorption
$N_O \to N_O+2$	$a_2 = \frac{1}{2}NP_Ok_O[S_O^{1\times2}(1-w)+S_O^{1\times1}w](1-u)^2(1-v)^2$	O_2 adsorption
$N_{CO} \to N_{CO}-1$	$a_3 = N[k_{des}^{1\times2}(1-w)+k_{des}^{1\times1}w]u$	CO desorption
$N_{CO} \to N_{CO}-1, N_O \to N_O-1$	$a_4 = Nk_{re}uv$	Reaction
$N_{1\times1} \to N_{1\times1}+1$	$a_5 = Nk_{1\times1}(1-w)\times f_{1\times1}(u,w)$, with $f_{1\times1}(u,w) = (1-\varepsilon)u^{\lambda}+\varepsilon w^{\lambda}$	(1×2) to (1×1)
$N_{1\times1} \to N_{1\times1}-1$	$a_6 = Nk_{1\times2}w\times f_{1\times2}(u,w)$, with $f_{1\times2}(u,w) = (1-\varepsilon)(1-u)^{\lambda}+\varepsilon(1-w)^{\lambda}$	(1×1) to (1×2)

oxygen atoms, and adsorption sites in a non-reconstructed (1×1) surface, respectively. According to these mechanisms, there are six reaction channels as listed in Table I and the meanings of the corresponding physical quantities are listed in Table II, where we have used $\mathbf{x} = (u, v, w)$ to stand for the concentrations of $(N_{CO}(t), N_O(t), N_{1\times1}(t))$. Note that the transition rates $a_{i=1,\ldots,6}$ are all proportional to the system size N.

According to the stochastic processes and transition rates shown in Table I , the CLE for the current model reads

$$\begin{aligned}\frac{du}{dt} &= \frac{1}{N}[(a_1-a_3-a_4)\\ &\quad +\sqrt{a_1}\eta_1(t)-\sqrt{a_3}\eta_3(t)-\sqrt{a_4}\eta_4(t)],\\ \frac{dv}{dt} &= \frac{1}{N}[(2a_2-a_4)+2\sqrt{a_2}\eta_2(t)-\sqrt{a_4}\eta_4(t)],\\ \frac{dw}{dt} &= \frac{1}{N}[(a_5-a_6)+\sqrt{a_5}\eta_5(t)-\sqrt{a_6}\eta_6(t)],\end{aligned} \quad (1)$$

where $\eta_{i=1,\ldots,6}(t)$ are Gaussian white noises with $\langle\eta_i(t)\rangle = 0$ and $\langle\eta_i(t)\eta_j(t')\rangle = \delta_{ij}\delta(t-t')$. The items with $\eta_i(t)$ give the internal noises, which scale as $1/\sqrt{N}$ because of $a_{i=1,\ldots,6} \propto N$. In the macroscopic limit $N\to\infty$, the internal noise items can be ignored and the system's dynamics is described by the deterministic equation,

$$\dot{x}_j = \frac{1}{N}\sum_{\rho=1}^{M}\nu_\rho^j a_\rho(\mathbf{x}) \equiv f_j(\mathbf{x}) \quad (x_{j=1,2,3} = u, v, w), \quad (2)$$

where $\nu_1 = (1,0,-1,-1,0,0)^T$, $\nu_2 = (0,2,0,-1,0,0)^T$, $\nu_3 = (0,0,0,0,1,-1)^T$, and $M=6$ is the number of reaction channels.

TABLE II. The meaning of physical quantities in Table I.

P_{CO}, P_O	Partial pressure in gas phase
k_{CO}, k_O	Impingement rate
$k_{des}^{1\times1}, k_{des}^{1\times2}$	Desorption rate of CO on 1×1 and 1×2 surface, respectively
k_{re}	Reaction rate
$k_{1\times1}$	Phase transition rate from 1×1 to 1×2
$S_{CO}, S_O^{1\times1}, S_O^{1\times2}$	Sticking coefficient
ξ	Precursor exponent
λ	Exponent
ε	Weight

The Fokker-Planck equation (FPE) corresponding to Eq. (1) reads

$$\begin{aligned}\frac{\partial p(\mathbf{x};t)}{\partial t} &= -\sum_i \frac{\partial}{\partial x_i}[f_i(\mathbf{x})p(\mathbf{x};t)]\\ &\quad +\frac{1}{2N}\sum_{i,j}\frac{\partial^2}{\partial x_i\partial x_j}[G_{ij}(\mathbf{x})p(\mathbf{x};t)],\end{aligned} \quad (3)$$

where $p(\mathbf{x};t)$ is the probability distribution in the concentration space, $f_j(\mathbf{x})$ is the deterministic term defined in Eq. (2), and $G_{ij}(\mathbf{x}) = 1/N\sum_{\rho=1}^{M}\nu_\rho^i\nu_\rho^j a_\rho(\mathbf{x})$. By introducing probability current density

$$J_i(\mathbf{x}) = \frac{1}{2}\sum_j G_{ij}\left(H_j - \frac{1}{N}\frac{\partial}{\partial x_j}\right)p(\mathbf{x};t), \quad (4)$$

where $H_j = 2\sum_k \Gamma_{jk}\tilde{f}_k$ with $\sum_j G_{ij}\Gamma_{jk} = \delta_{ik}$ and $\tilde{f}_k = f_k - 1/(2N)\sum_j \partial G_{kj}/\partial x_j$, we can write the FPE in a compact form $\partial_t p(\mathbf{x};t) = -\sum_i \partial J_i/\partial x_i$.

With the variation of the parameters P_O and P_{CO}, the system (2) shows very abundant bifurcation features.[17,50] In the present paper, we fix $P_O = 9.6\times10^{-5}$ mbar, $T = 520$ K and choose P_{CO} as the only control parameter. In such a case, the bifurcation diagram of the deterministic system (2) is shown in Fig. 1. There is a supercritical HB at $P_{CO} \simeq 3.557\times10^{-5}$, where a stable limit cycle emerges. The limit cycle disappears via a saddle-node infinite period (SNIPER) bifurcation when it encounters the turning point (TP1) at $P_{CO} \simeq 3.6151\times10^{-5}$. For P_{CO} less than HB or larger than TP1, the system only shows one stable state. Stable oscillations can only be observed in the region between HB and TP1. In addition, an interesting feature of the system is the existence of a CANARD point at $P_{CO} \simeq 3.575\times10^{-5}$, where a very fast transition from a small amplitude oscillation to a large amplitude oscillation occurs.[51]

In Fig. 2, typical stochastic oscillations for four different system sizes are shown. For $N = 10^8$, the internal noise is rather small and the dynamics of system approximately obeys the deterministic Eq. (2), hence the CO concentration only shows slight fluctuations around the deterministic steady state as shown in the bottom panel. When the system size decreases to a smaller value, e.g., $N = 10^6$, random fluctuation around the steady state changes to "stochastic oscillation" with small amplitude. With further decreasing of the system size, we find that occasional random pulses are triggered on the

Downloaded 23 May 2013 to 129.186.1.55. This article is copyrighted as indicated in the abstract. Reuse of AIP content is subject to the terms at: http://jcp.aip.org/about/rights_and_permissions

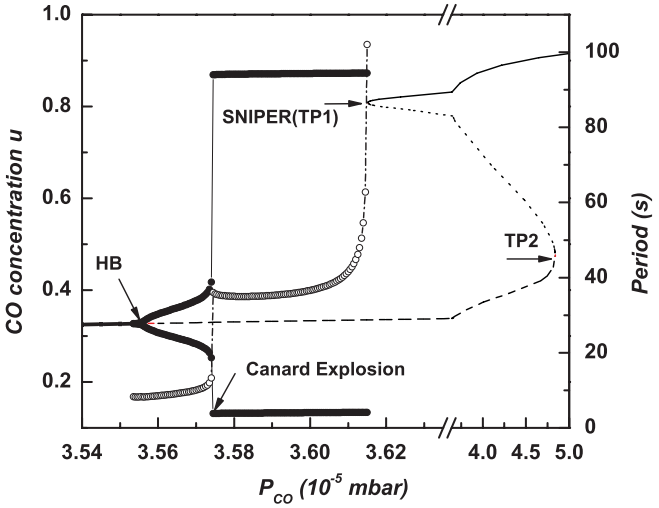

FIG. 1. Bifurcation diagram for the deterministic system (2). HB stands for the supercritical Hopf bifurcation at $P_{\rm CO} \simeq 3.557 \times 10^{-5}$, TP1 and TP2 denote two turning points at $P_{\rm CO} \simeq 3.6151 \times 10^{-5}$ and $P_{\rm CO} \simeq 4.839 \times 10^{-5}$, respectively. Stable limit cycles exist in the region between HB and TP1, where the solid circles show the concentration range of the oscillations. Note the oscillation ends at TP1 via a SNIPER bifurcation. The heavy solid lines denote stable steady states, the dashed line unstable states, and the dotted line saddle states. The dependence of the oscillation period between HB and TP1 is depicted by the open circles (the right axis). Importantly, there is a CANARD point at $P_{\rm CO} \simeq 3.575 \times 10^{-5}$. The bifurcation diagram is calculated by use of the BIFPACK software (Ref. 52).

background of the small stochastic oscillations. For an optimal cell size, $N = 10^4$ for instance, the pulse can become rather regular.

To apply the ST of this excitable system, we now consider a path $\chi(t)$ generated by Eq. (1) starting from $\mathbf{x}_0(\tau = 0)$ selected from some normalized distribution $p_0(\mathbf{x}_0)$ and ending at $\mathbf{x}_t(\tau = t)$ with normalized distribution $p_1(\mathbf{x}_t)$. Correspondingly, the time-reversed path $\tilde{\chi}(t)$ starts from $\tilde{\mathbf{x}}_0 = \mathbf{x}_t$ and ends at $\tilde{\mathbf{x}}_t = \mathbf{x}_0$ with $\tilde{\mathbf{x}}(\tau) = \mathbf{x}(t - \tau)$. According to Seifert,[2] one may define the system entropy along this single trajectory as

$$S(\tau) = -lnp(\mathbf{x}(\tau), \tau), \tag{5}$$

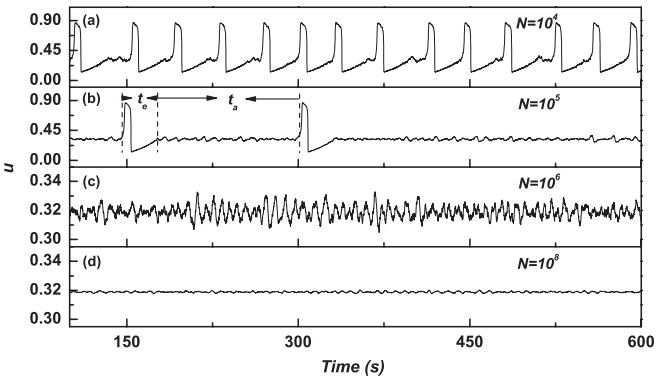

FIG. 2. Typical time series of CO concentration for different system sizes N at $P_{\rm CO} = 3.55 \times 10^{-5}$ mbar. From top to bottom, N reads 10^4, 10^5, 10^6, and 10^8, respectively. Note that the vertical axis has different scales in panels (a) and (b) from those in (c) and (d). For relatively small N, the stochastic oscillations are of large amplitude, while for large N, the amplitude is small. For $N \sim 10^5$, neither type of stochastic oscillations dominates. In panel (b), t_a and t_e denote the activation and excursion time periods, respectively.

where $p(\mathbf{x}(\tau), \tau)$ is the solution of the Fokker-Planck equation evaluated along the trajectory at time τ. As shown in Ref. 26, by evaluating the entropy balance along the trajectory, one may calculate the so-called "medium" entropy change as follows:

$$\Delta s_m = V \int_0^t dt \sum_i H_i \dot{x}_i, \tag{6}$$

where $\dot{x}_i$ is evaluated along $\chi(t)$. It can be shown that the total entropy change along the path $\Delta s_{tot} = \Delta s_m + \Delta s$ obeys the second-law like inequality $\Delta s_{tot} \geq 0$ and integral FT $\langle e^{-\Delta s_{tot}} \rangle = 1$.[2] In the stationary state, a detailed FT $p(\Delta s_{tot})/p(-\Delta s_{tot}) = e^{\Delta s_{tot}}$ also holds. Note that for long time trajectories, Δs only contributes a boundary term to Δs_{tot} and is much smaller than Δs_m, one expects that both types of FT also hold approximately for Δs_m. We can use the time-averaged entropy production P to measure the dynamic dissipation rate

$$P \equiv lim_{t\to\infty} \frac{\langle \Delta s_m \rangle}{t} = V \sum_i \langle\langle H_i \dot{x}_i \rangle\rangle_s, \tag{7}$$

where $\langle\langle \cdot \rangle\rangle_s$ means averaging over both time and the stationary distribution. We will mainly investigate how P depends on the system size N and the control parameter $P_{\rm CO}$.

In this study, 10^5 stationary trajectories with length $t = 0.5$ are generated to calculate the distribution of medium entropy change Δs_m via Eq. (6). The results are plotted in Fig. 3 for different $P_{\rm CO}$ with fixed system size $N = 2 \times 10^5$. It is noted that the distributions are strongly non-Gaussian. Apparently, the distribution shows no significant difference when the control parameter increases from the steady state region to the oscillation region, and neither the Hopf bifurcation nor the CANARD explosion plays any role here. We note here that the ensemble average of Δs_m is quite large here, and the probabilities of paths with negative Δs_m are fairly small. If we want to verify the detailed FT $p(\Delta s_m)/p(-\Delta s_m) = e^{\Delta s_m}$ or integral FT $\langle e^{-\Delta s_m} \rangle = 1$ here, much more realizations of Δs_m are required.

To quantify the dissipation of the system, the mean entropy production P is calculated according to Eq. (7). As shown in Fig. 4, we have considered the effects of system size N and control parameter $P_{\rm CO}$. Several interesting features can be observed. For $P_{\rm CO}$ in the steady region, e.g., $P_{\rm CO} = 3.55 \times 10^{-5}$ and 3.555×10^{-5}, scaling law $P \propto N^0$ is observed in the large system size (weak noise) limit, which is in accordance with the prediction of our previous studies.[26] In addition, it is noted that P could scale as $P \propto N^1$ in the small system size (large noise) limit. More interestingly, P shows a clear-cut maximum at some optimal system size. For $P_{\rm CO}$ between the HB and CANARD, where the deterministic system shows small-amplitude oscillation, e.g., $P_{\rm CO} = 3.56 \times 10^{-5}$ and 3.565×10^{-5}, P scales as N^1 for both small and large N, while a maximum still appears at some intermediate N. The scaling for large N is also in agreement with the results in Ref. 26. For $P_{\rm CO}$ very close to the CANARD, e.g., $P_{\rm CO} = 3.573 \times 10^{-5}$, it seems that the maximum moves to very large N. For $P_{\rm CO}$ on the right side of the CANARD where deterministic large amplitude

Downloaded 23 May 2013 to 129.186.1.55. This article is copyrighted as indicated in the abstract. Reuse of AIP content is subject to the terms at: http://jcp.aip.org/about/rights_and_permissions

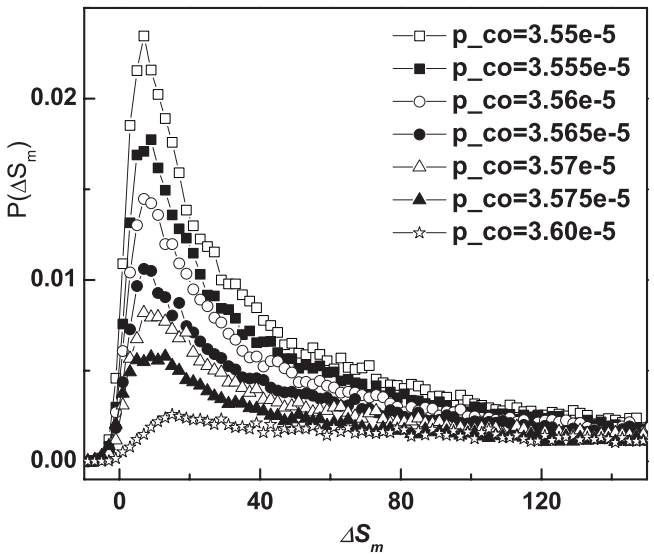

FIG. 3. Typical distribution $p(\Delta s_m)$ of the medium entropy change Δs_m in different parameter regions. System size is $N = 2 \times 10^5$.

relaxation oscillations are observed, e.g., $P_{\mathrm{CO}} = 3.577 \times 10^{-5}$ and 3.60×10^{-5}, P scales as N^1 in the whole range of N and the maximum disappears. In this relaxation oscillation region, P is not sensitive to the bifurcation parameter P_{CO}. We note that such nontrivial behaviors are quite different from the system we studied in Ref. 26, where no excitability exists. Intuitively, one expects that these features must be relevant to the noise-induced dynamics of such a system.

Although the normal form analysis presented in our previous work[26] can reasonably address the scaling of P for large N for P_{CO} near the HB, it cannot explain the appearance of the maximum and the scaling for P_{CO} in the relaxation region. Here, we try to give a qualitative discussion. As shown in Fig. 2, each stochastic trajectory can be divided into two parts of segments: one consists of the small amplitude oscillations during the activation time t_a, the other contains the spikes (relaxation oscillations with large amplitude) during the excursion time t_e. If we define the factor $\alpha \equiv \langle t_e \rangle / (\langle t_a \rangle + \langle t_e \rangle)$ as the time percentage of spikes in the trajectory, then one may write

$$P = [\alpha P_1 + (1 - \alpha) P_2], \tag{8}$$

where P_1 and P_2 are the mean entropy production corresponding to the spikes and small amplitude oscillations, respectively. We can separately investigate the dependences of P_1, P_2 and α on the system size N, thus may provide a reasonable explanation to the curves in Fig. 4.

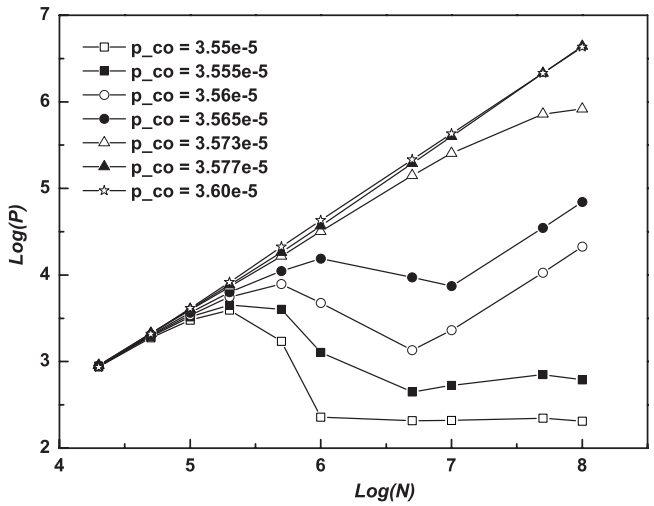

FIG. 4. Dependence of the mean entropy production P on the system size N for different P_{CO}.

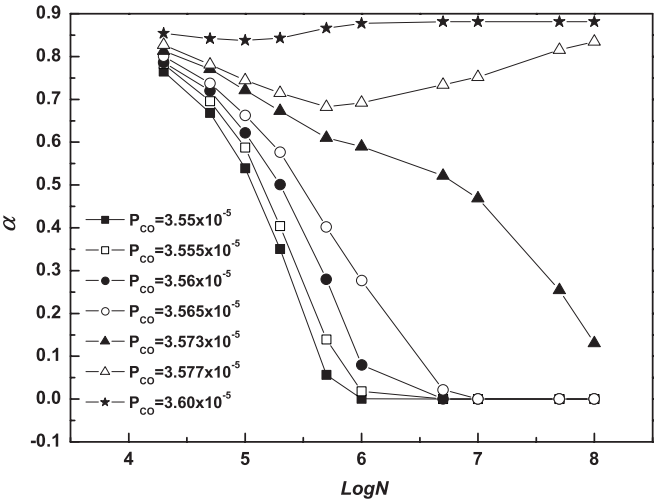

FIG. 5. Dependence of the time percentage factor α on system size N for different P_{CO}.

In Fig. 5, we have plotted the dependence of α on N for different P_{CO} as those in Fig. 4. Clearly, two distinct types of tendency can be observed. For P_{CO} less than the CANARD, α decreases quickly to nearly zero as N becomes large. In this region, the system is excitable, and the spike occurs via some type of barrier crossing, and α is related to the first passage time for such an escape problem. Assume that the barrier height is not dependent on the system size N, and notice that the $1/N$ measures the level of internal noise, one may assert that $\alpha \propto e^{-bN}$, where b is a constant not dependent on N. However, the fitting is not good for the data shown in Fig. 5, indicating that the dynamics is much more complex. For P_{CO} larger than the CANARD, one can see that α is close to 1, and not sensitive to the system size N. This is reasonable because the deterministic system already shows spikes in this parameter region. In Fig. 6, P_1 and P_2 are presented as functions of N, where they show distinct features. The curves for P are also presented for comparison. The main observation is that P_1 is always proportional to N, no matter where P_{CO} is, and it is always much larger than P_2. The behavior of P_2 depends on the parameter P_{CO}: for $P_{\mathrm{CO}} >$ HB, see panels (c) to (f), P_2 also increases linearly with N; but for $P_{\mathrm{CO}} <$ HB, P_2 scales as N^1 when N is small and N^0 when N is large.

Combine above features, one may qualitatively understand the nontrivial behaviors of P shown in Fig. 4 as follows:

1. For $P_{\mathrm{CO}} >$ CANARD, the deterministic system shows spikes. In this region, both P_1 and P_2 are proportional to

Downloaded 23 May 2013 to 129.186.1.55. This article is copyrighted as indicated in the abstract. Reuse of AIP content is subject to the terms at: http://jcp.aip.org/about/rights_and_permissions

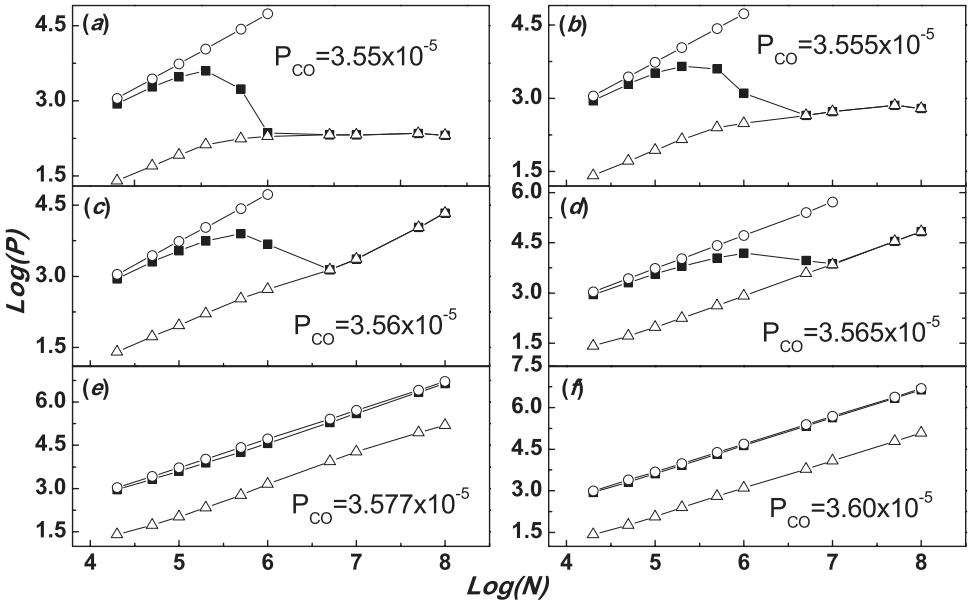

FIG. 6. The total entropy production P(■), that of spikes P_1(○), and of small oscillations P_2(△) are plotted as functions of the system size N for different control parameter P_{CO}.

N, and α is nearly one. Thus $P \sim P_1$ and it is naturally that $P \propto N^1$.

2. For $P_{CO} <$ HB, the deterministic system shows steady state. When N is large, α is nearly zero and $P \sim P_2$, leading readily to $P \propto N^0$. When N is small, noting that $\alpha \gg 1-\alpha$ and $P_1 \gg P_2$, we have $P \sim P_1$, which is in accordance with the linear relationship. In the intermediate N region, one may write $P_1 \sim c_1 N$, $P_2 \sim c_2 N$, $\alpha \sim e^{-bN}$, where $c_1 > c_2 > 0$ and $b > 0$ are constants. Summing these terms together, it is easy to show that a maximum arises at some optimal value of N.
3. For P_{CO} between the HB and the CANARD, the deterministic system shows small amplitude oscillation but no spikes. In this region, both P_1 and P_2 are also both proportional to N, which is similar to the case when P_{CO} is larger than the CANARD. Thus in the large N limit, P is mainly contributed by P_2 and should be linearly dependent on N. The same reasoning as in item 2 for $P_{CO} <$ HB also holds here, which may qualitative illustrate the linear dependence in the small N range and the occurrence of extreme in the intermediate N range.

III. CONCLUSIONS

In summary, we have applied the concepts and principles of ST to a mesoscopic chemical oscillation system with both oscillatory and excitable dynamics. The multiscale nature of the system and the existence of a CANARD lead to interesting noise-induced dynamics. Generally, a stochastic trajectory contains of a number of spikes lying on the background of small amplitude oscillations. We find that the time-averaged entropy productions, contributed from the spikes or from the small oscillations, show quite different dependences on the system size. This also leads to nontrivial dependence of the total entropy production on the system size, even including a maximum for certain control parameters. This work thus unravels the very relationship between the noisy dynamics of a stochastic system and ST features. Since excitable systems with oscillatory dynamics are ubiquitous in many chemical, biological, and physical disciplines, our study could open more perspectives regarding the application of ST.

ACKNOWLEDGMENTS

This work is supported by the National Science Foundation of China (Grant Nos. 20873130, 20933006).

[1] U. Seifert, J. Phys. A **37**, L517 (2004).
[2] U. Seifert, Phys. Rev. Lett. **95**, 040602 (2005).
[3] U. Seifert, Eur. Phys. J. B **64**, 423 (2008).
[4] C. Tietz, S. Schuler, T. Speck, U. Seifert, and J. Wrachtrup, Phys. Rev. Lett. **97**, 050602 (2006).
[5] V. Blickle, T. Speck, L. Helden, U. Seifert, and C. Bechinger, Phys. Rev. Lett. **96**, 070603 (2006).
[6] T. Schmiedl and U. Seifert, J. Chem. Phys. **126**, 044101 (2007).
[7] T. Schmiedl, T. Speck, and U. Seifert, J. Stat. Phys. **128**, 77 (2007).
[8] M. A. Leontovich, Zhurnal Teoret. Ehksper. Fiziki **5**, 211 (1935), (in Russian).
[9] M. Delbrück, J. Chem. Phys. **8**, 120 (1940).
[10] D. A. McQuarrie, J. Appl. Probab. **4**, 245 (1967); *Stochastic Approach to Chemical Kinetics* (Methuen, London, 1968).
[11] I. Oppenheim, K. E. Shuler, and G. H. Weiss, *Stochastic Processes in Chemical Physics: The Master Equations* (MIT Press, Cambridge, MA, 1977); P. Hanggi, K. E. Shuler, and I. Oppenheim, Physica A **107**, 143 (1981).
[12] N. G. van Kampen, Adv. Chem. Phys. **34**, 245 (1976); *Stochastic Processes in Physics and Chemistry* (North-Holland, Amsterdam, 1981).
[13] T. G. Kurtz, Math. Prog. Study **5**, 67 (1976); Stochastic Proc. Appl. **6**, 223 (1978).
[14] P. Érdi and J. Tóth, *Mathematical Models of Chemical Reactions: Theory and Applications of Deterministic and Stochastic Models* (Manchester University Press, Manchester, UK, 1989).
[15] D. T. Gillespie, J. Comput. Phys. **22**, 403 (1976); Annu. Rev. Phys. Chem. **58**, 35 (2007).
[16] M. Vellela and H. Qian, J. R. Soc., Interface **6**, 925 (2009).
[17] C. Reichert, J. Starke, and M. Eiswirth, J. Chem. Phys. **115**, 4829 (2001).
[18] J. Keizer, *Statistical Thermodynamics of Nonequilibrium Processes* (Springer-Verlag, New York, 1987).

Downloaded 23 May 2013 to 129.186.1.55. This article is copyrighted as indicated in the abstract. Reuse of AIP content is subject to the terms at: http://jcp.aip.org/about/rights_and_permissions

[19]G. Nicolis and I. Prigogine, *Self-Organization in Nonequilibrium Systems: From Dissipative Structures to Order through Fluctuations* (Wiley, New York, 1977); L. Jiu-Li, C. Van den Broeck, and G. Nicolis, Z. Phys. B: Condens. Matter **56**, 165 (1984).
[20]P. Gaspard, J. Chem. Phys. **120**, 8898 (2004).
[21]D. Andrieux and P. Gaspard, J. Chem. Phys. **121**, 6167 (2004).
[22]D. Andrieux and P. Gaspard, J. Stat. Mech: Theory Exp. 01011 (2006).
[23]D. Andrieux and P. Gaspard, J. Chem. Phys. **128**, 154506 (2008).
[24]D. Andrieux and P. Gaspard, Phys. Rev. E **77**, 031137 (2008).
[25]T. J. Xiao, Z. H. Hou, and H. W. Xin, J. Chem. Phys. **129**, 114506 (2008).
[26]T. J. Xiao, Z. H. Hou, and H. W. Xin, J. Phys. Chem. B **113**, 9316 (2009).
[27]Z. H. Hou, T. J. Xiao, and H. W. Xin, Chem. Phys. Chem. **7**, 1520 (2006).
[28]T. J. Xiao, J. Ma, and Z. H. Hou, New J. Phys. **9**, 403 (2007).
[29]A. S. Mikhailov and G. Ertl, Chem. Phys. Chem. **10**, 86 (2009).
[30]Y. De Decker and A. S. Mikhailov, Prog. Theor. Phys. Suppl. **165**, 119 (2006).
[31]C. Sachs, M. Hildebrand, S. Volkening, J. Wintterlin, and G. Ertl, Science **293**, 1635 (2001).
[32]T. Zambelli, J. V. Barth, J. Wintterlin, and G. Ertl, Nature (London) **390**, 495 (1997).
[33]S. Jakubith, H. H. Rotermund, W. Engel, A. von Oertzen, and G. Ertl, Phys. Rev. Lett. **65**, 3013 (1990).
[34]J. M. Davidenko, A. V. Pertsov, R. Salomonsz, W. Baxter, and J. Jalife, Nature (London) **355**, 349 (1992).
[35]Y. Suchorski, J. Beben, E. W. James, J. W. Evans, and R. Imbihl, Phys. Rev. Lett. **82**, 1907 (1999); Y. Suchorski, J. Beben, and R. Imbihl, Prog. Surf. Sci. **59**, 343 (1998).
[36]A. T. Bell, Science **299**, 1688 (2003).
[37]N. V. Peskov, M. M. Slinko, and N. I. Jaeger, J. Chem. Phys. **116**, 2098 (2002).
[38]V. Gorodetskii, W. Drachsel, and J. H. Block, Catal. Lett. **19**, 223 (1993); V. K. Medvedev, Yu. Suchorski, and J. H. Block, Appl. Surf. Sci. **76/77**, 136 (1994); V. Gorodeskii, N. Ernst, W. Drachsel, and J. H. Block, *ibid.* **87/88**, 151 (1995); V. K. Medvedev, Yu. Suchorski, and J. H. Block, *ibid.* **94/95**, 200 (1996).
[39]C. Voss and N. Kruse, Appl. Surf. Sci. **94/95**, 186 (1996).
[40]Y. Suchorski, R. Imbihl, and V. K. Medvedev, Surf. Sci. **401**, 392 (1998).
[41]V. Johanek, M. Laurin, A. W. Grant, B. Kasemo, C. R. Henry, and J. Libuda, Science **304**, 1639 (2004).
[42]N. I. Jaeger, N. V. Peskov, and M. M. Slinko, Kinetics and Catalysis **44**, 183 (2003).
[43]N. V. Peskov, M. M. Slinko, and N. I. Jaeger, Chem. Eng. Sci. **58**, 4797 (2003).
[44]D. J. Liu and J. W. Evans, Phys. Rev. B **75**, 073401 (2007).
[45]R. M. Eiswirth, K. Krischer, and G. Ertl, Appl. Phys. A **51**, 79 (1990).
[46]M. Eiswirth, M. Bar, and H. H. Rotermund, Physica D **84**, 40 (1995).
[47]J. Starke, C. Reichert, M. Eiswirth, H. H. Rotermund, and G. Ertl, Europhys. Lett. **73**(6), 820 (2006).
[48]M. Kim, M. Bertram, M. Pollmann, A. von Oertzen, A. S. Mikhailov, H. H. Rotermund, and G. Ertl, Science **292**, 1357 (2001).
[49]M. M. Slinko, A. A. Ukharskii, N. V. Peskov, and N. I. Jaeger, Catal. Today **70**, 341 (2001).
[50]Z. H. Hou, T. Rao, and H. W. Xin, J. Chem. Phys. **122**, 134708 (2005).
[51]M. Brøns and K. Bar-Eli, J. Phys. Chem. **95**, 8706 (1991); M. Krupa and P. Szmolyan, J. Differ. Equations **174**, 312 (2001); H. G. Rotstein, N. Korpell, A. M. Zhabotinsky, and I. R. Epstein, J. Chem. Phys. **119**, 8824 (2003); SIAM J. Appl. Math. **63**, 1998 (2003).
[52]*Practical Bifurcation and Stability Analysis: From Equilibrium to Chaos*, 2nd ed., edited by R. Seydel (Springer, Berlin, 1999); see http://www.bifurcation.de/software.html.

Downloaded 23 May 2013 to 129.186.1.55. This article is copyrighted as indicated in the abstract. Reuse of AIP content is subject to the terms at: http://jcp.aip.org/about/rights_and_permissions